Lawrence Berkeley National Laboratory
Chemical Sciences

Title
Competitive Coordination Strategy to Finely Tune Pore Environment of Zirconium-Based Metal–Organic Frameworks

Authors
He, Ting
Ni, Bing
Xu, Xiaobin
et al.

Competitive Coordination Strategy to Finely Tune Pore Environment of Zirconium-Based Metal–Organic Frameworks

Ting He,[†,‡,§] Bing Ni,[‡] Xiaobin Xu,[‡] Haoyi Li,[‡] Haifeng Lin,[‡] Wenjuan Yuan,[⊥] Jun Luo,[⊥] Wenping Hu,[†] and Xun Wang*[,‡]

[†]Department of Chemistry, School of Science, Tianjin University, Tianjin 300072, China
[‡]Key Lab of Organic Optoelectronics and Molecular Engineering, Department of Chemistry, Tsinghua University, Beijing 100084, China
[§]School of Chemistry and Chemical Engineering, Qinghai Normal University, Xining 810000, China
[⊥]School of Materials Science and Engineering, Tianjin University of Technology, Tianjin 300384, China

S *Supporting Information*

ABSTRACT: Metal–organic frameworks (MOFs) are a class of crystalline porous materials with reticular architectures. Precisely tuning pore environment of MOFs has drawn tremendous attention but remains a great challenge. In this work, we demonstrate a competitive coordination approach to synthesize a series of zirconium–metalloporphyrinic MOFs through introducing H_2O and monocarboxylic acid as modulating reagents, in which well-ordered mesoporous channels could be observed clearly under conventional transmission electron microscopy. Owing to plenty of unsaturated Lewis acid catalytic sites exposed in the visualized mesoporous channels, these structures exhibit outstanding catalytic activity and excellent stability in the chemical fixation of carbon dioxide to cyclic carbonates. The zirconium-based MOFs with ordered channel structures are expected to pave the way to expand the potential applications of MOFs.

zirconium metalloporphyrin-MOFs
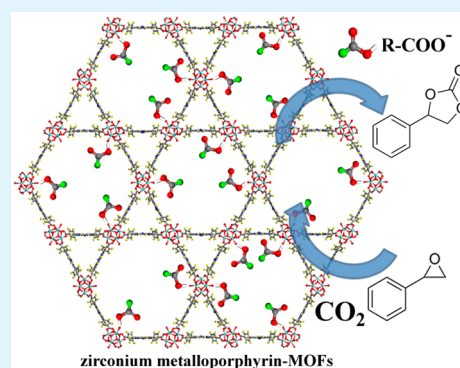
INTRODUCTION

The idea of reticular chemistry which is concerned with repeated linking of inorganic clusters and other molecular building blocks has made the construction of metal–organic frameworks (MOFs) flourish. MOFs, which are constructed with metal ions and organic linkers with tunable porous structures, have received tremendous attention[1−4] because of their potential applications in catalysis,[5,6] separations,[7] gas storage,[8] drug delivery,[9] and so on.[10−14] MOFs are considered as a type of ideal crystalline material in that all metal ions are coordinated by the organic linkers at fixed positions in a periodical lattice in exactly the same environments. Interestingly, recent studies demonstrate that plenty of structural defects and local disorders are present in MOFs, while the robustness and structural integrity of the framework are retained.[15−17]

Focusing on the relationship between the structure and function of MOFs at the molecular level, controllable tuning of their internal surface areas and pore environment have been proven to endow them with desirable chemical functionality.[18,19] Recently, some efforts have been devoted to introducing monocarboxylic acid (modulating reagent) to the synthesis of Uio-66 ($Zr_6(OH)_4O_4(BDC)_6$; BDC = benzene-1,4-dicarboxylate) to tailor the pore environment and form

missing links (defects), which have a beneficial effect on their catalytic activity,[20] porosity,[21] and stability.[22] We have also proposed a competitive coordination strategy to tune the local chemical environments. As a proof of concept, hierarchical porous MOFs with both micro- and mesopores are synthesized through an etching process tuned by a competitive ligand.[23] It seems that the nuance in local chemical environment has profound impact on performance. Nevertheless, precisely controlling the internal environment of porous channels for long range in MOFs remains synthetically challenging. Moreover, detection of minute local disorder in the chemical environment is rather challenging because signals of such disorder in conventional characterizations are usually obscured due to the low content.

Herein, we developed a competitive coordination strategy to synthesize a series of zirconium–metalloporphyrinic MOFs with well-ordered mesoporous structures (WM-MOFs) by introducing trace water and modulating reagents into the reaction system to tune the pore environment of WM-MOFs, and the robustness of pores was qualified by conventional
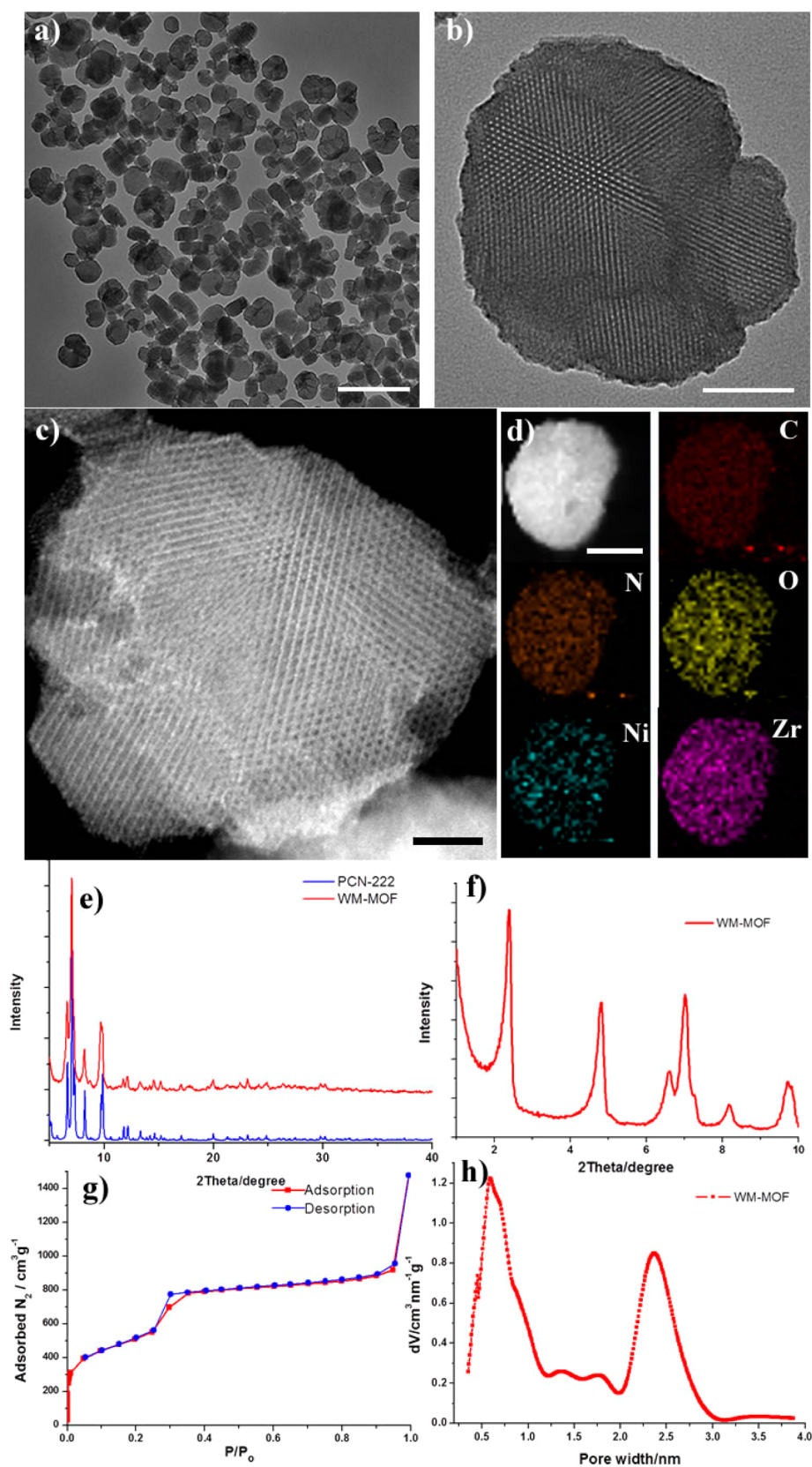
Figure 1. (a and b) TEM (a: scale bar 500 nm; b: scale bar 50 nm), (c) HAADF-STEM (scale bar 20 nm), (d) EDX elemental mapping (scale bar 50 nm), (e) PXRD pattern, (f) SAXS pattern, (g) nitrogen adsorption (squares) and desorption (circles) isotherms measured at 77 K, and (h) pore size distribution.

transmission electron microscopy (TEM) (actually, few frameworks have been imaged in their intact structure by

TEM using low dose conditions or special instruments[24−28] to the best of our knowledge). For WM-MOFs, the pores can be
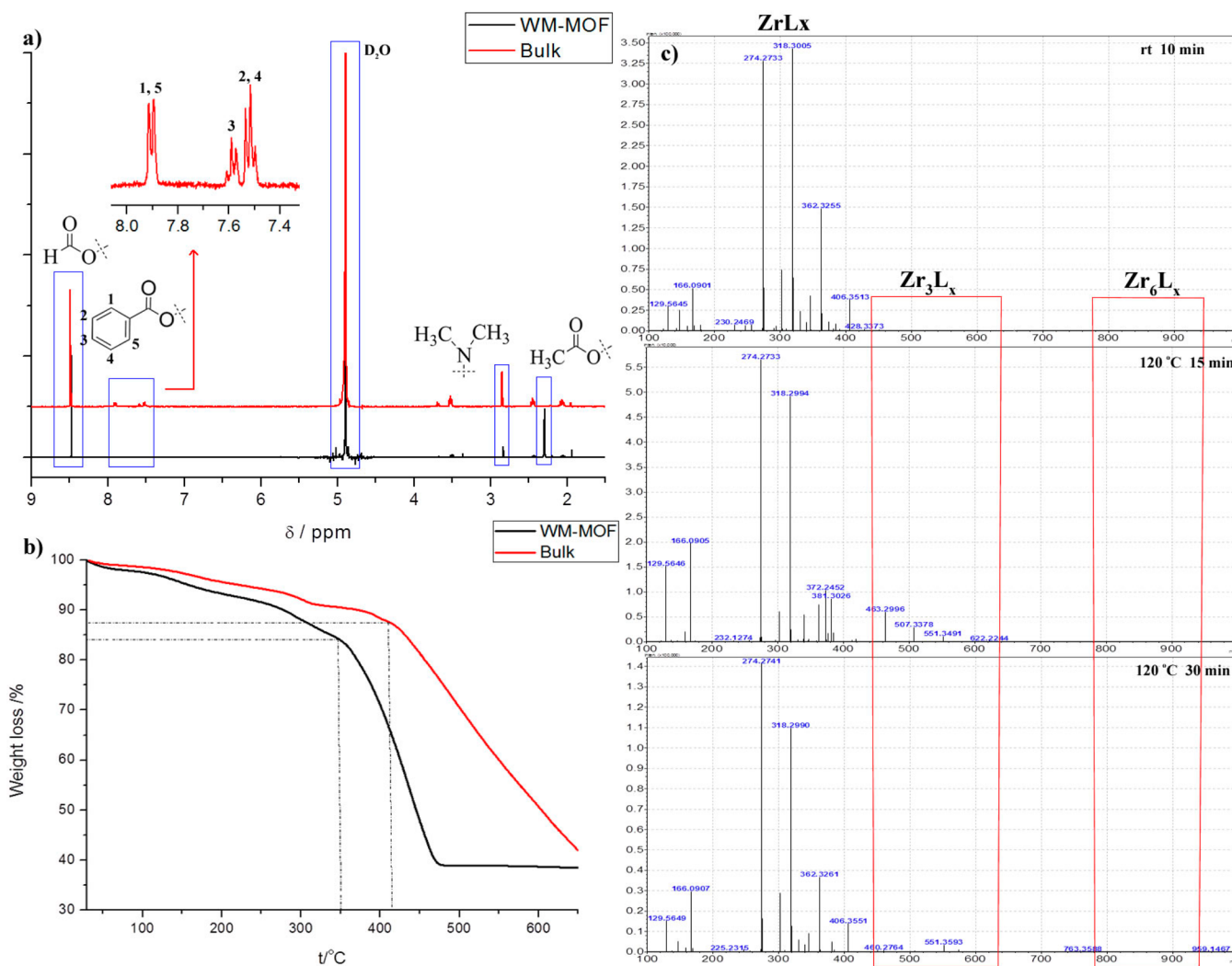
Figure 2. (a) Dissolution/^{1}H NMR spectra of WM-MOF and bulk samples, (b) TG curves taken in nitrogen of WM-MOF-AA and bulk samples, and (c) ESI-MS spectra of the WM-MOF reaction solutions at different times.

clearly seen under conventional TEM operated at an accelerating voltage of 100 kV and scanning TEM (STEM) operated at an accelerating voltage of 200 kV, while for counterparts, the pores cannot be clearly seen, though their X-ray diffraction (XRD) patterns all corresponded well with PCN-222. The thermogravimetric (TG) curve, dissolution/ nuclear magnetic resonance (NMR) spectrometry, and time dependent electrospray ionization-mass spectrometry (ESI-MS) provided significant information on the formation process and pore environment of MOFs, which demonstrated that pore environment can be modulated precisely. Taking advantage of the unique internal environment, high number of exposed catalytic active sites, and the gas adsorption capacity of WM-MOFs, these structures show highly enhanced catalytic performance in the cycloaddition of carbon dioxide and epoxides at ambient pressure compared to that of their counterparts.

RESULTS AND DISCUSSION

WM-MOFs were synthesized via a solvothermal reaction of zirconium chloride (ZrCl$_4$), nickel-tetrakis(4-carboxyphenyl)-porphyrin (Ni-TCPP), acetic acid (molar ratio of AA:Zr^{4+} = 50:1), and trace H$_2$O in N,N-dimethylformamide (DMF)

solvent. The porous morphology, composition, and structure were investigated by various characterization techniques. TEM (Figures 1a, 1b, and Figure S1) and high-angle annular dark-field scanning TEM (HAADF-STEM) (Figure 1c) images showed that the product was uniform and consisted of visualized and well-ordered mesoporous channels with an approximate diameter of 2.8 nm. As a comparison, bulk counterpart was synthesized by the reported method.[29] To our surprise, these long-range ordered channels were not observed directly in the bulk counterpart under TEM (Figure S2). This was the direct evidence of the different pore environment between WM-MOF and their respective parent frameworks due to the fact that powder XRD (PXRD) provided only an averaged picture. Elemental mapping spectra (Figure 1d) using energy-dispersive X-ray spectroscopy (EDX) demonstrated the homogeneous distribution of C, N, O, Ni, and Zr throughout the whole structure. The PXRD pattern (Figure 1e) of the sample corresponded well with the reported single crystals of PCN-222.[29] Meanwhile, the X-ray photoelectron spectra (XPS) confirmed the composition of the product (Figure S3). The small-angle X-ray scattering (SAXS) (Figure 1f) confirmed the mesoporous feature. The porosity was also analyzed by nitrogen adsorption–desorption isotherms and pore size distribution measurements (Figure 1g); nitrogen sorption
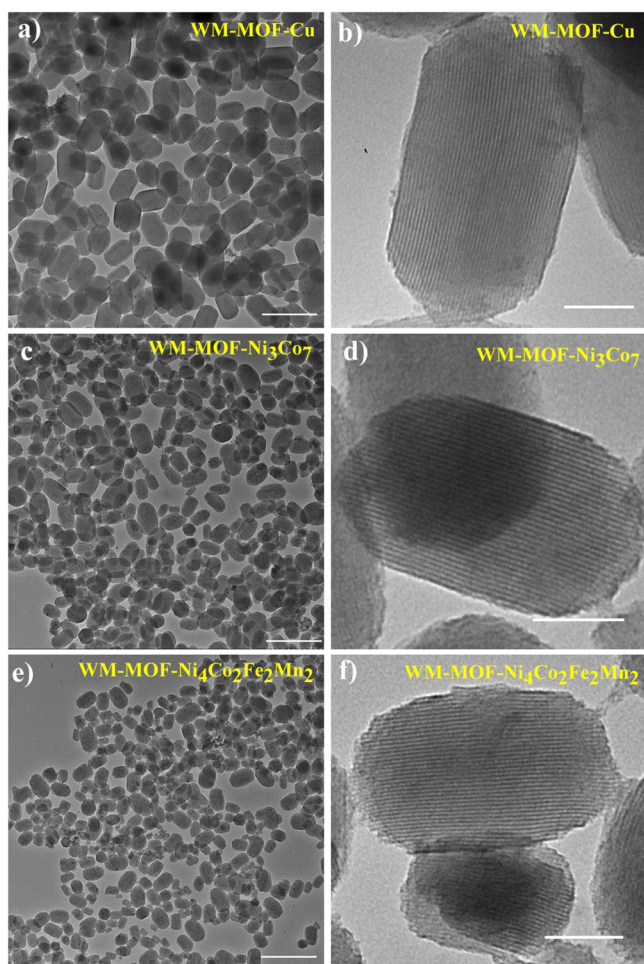
Figure 3. TEM images of WM-MOF-Cu (a and b), WM-MOF-Ni$_3$Co$_7$ (c and d), and WM-MOF-Ni$_4$Co$_2$Fe$_2$Mn$_2$ (e and f). scale bar: a−c, 500 nm; d−f, 50 nm.

data at 77 K displayed a typical type IV isotherm, suggesting the presence of mesopores. Pore size distribution was calculated from the Saito−Foley (SF) method (Figure 1h), indicating the existence of both micropores (0.6 nm) and mesopores (2.5 nm) simultaneously, which was in good agreement with the HAADF-STEM results. According to the nitrogen adsorption−desorption isotherms, the Brunauer−Emmett−Teller (BET) surface area and total pore volume were calculated to be 1724 m^2 g^{-1} and 2.283 cm^3 g^{-1}, respectively. Moreover, the atomic ratio of Zr/Ni in the WM-MOF was determined by inductively coupled plasma optical emission spectrometry (ICP-OES), and the measured value was 3.77:1 (Table S1). A series of 2D HAADF-STEM images were taken at consecutive tilt angles from −10° to 10° to verify the well-ordered mesoporous structure (Supplementary Movies 1 and 2). Impressively, WM-MOFs exhibited extraordinary stability. As confirmed by TEM images and XRD patterns, no structure collapse or phase transition happened when immersing samples in water or even strongly acidic (pH 0) or basic (pH 12) aqueous solutions for 24 h (Figures S4 and S5).

To further acquire insight into the formation of WM-MOFs, a series of control experiments was carried out. TEM images (Figures S6a−c) showed that trace H$_2$O was indispensable to the construction of visualized well-ordered mesoporous nanostructures, which was in accordance with PXRD results

(Figure S7). The amount of H$_2$O should be carefully adjusted: low-crystallinity particles were obtained without H$_2$O (Figure S6a), while an excess amount of H$_2$O resulted in structural destruction and low crystallinity (Figure S6c). The dissolution/NMR spectroscopy was conducted to identify the impact of modulating reagents on pore environment of samples. The WM-MOFs and bulk counterparts were digested in 1 M NaOH (in D$_2$O) and recorded by ^{1}H NMR (Figure 2a). The single peak at 2.3 ppm of WM-MOFs and 3 peaks at 7.5 to 8.0 ppm of bulk counterparts were surely assigned to acetate and benzoate, respectively, which were in accordance with the synthetic conditions (acetic acid act as modulating reagent for WM-MOFs and benzoic acid for bulk counterparts). The signals at 8.5 and 2.8 ppm could be assigned to formate and N,N-dimethyl fragments, which originated from DMF hydrolysis during synthesis and activation procedures. The loss of porphyrinic acid peaks was due to the insolubility in D$_2$O. Due to the rigorous activation procedure for samples (Experimental Section), we were confident that all detected signals of monocarboxylates were incorporated into the MOF structure. The chemical composition and environment of the internal pore were indeed tuned by the modulating reagents. The thermogravimetric curves taken in nitrogen (air) are presented in Figure 2b and Figure S8. For WM-MOFs, the weight loss of about 26% over a temperature range of 25−350 °C represented the removal of H$_2$O and modulating reagent, and the framework began to collapse at 350 °C. In contrast, bulk counterparts showed lower weight loss of small molecules (22%) and better thermal stability (420 °C). In the prototypical PCN-222 structure, eight edges of Zr$_6$(OH)$_8$ core were bridged by carboxylates, and remaining four positions were occupied by terminal hydroxy groups.[29] When trace H$_2$O and excess acetic acid were introduced into the synthesis system, more modulating reagent coordinated with nodes through the competitive coordination procedure, and the Zr clusters reduced linker connectivity while the familiar geometry of PCN-222 was maintained. The effect of H$_2$O was significant during this process: (1) accelerating hydrolysis of zirconium salt to promote crystal nucleation and inhibiting growth; (2) facilitating deprotonation of acid, where the excess modulating reagent dominates the competition for Zr clusters; and (3) excess H$_2$O leading to much less ligand incorporating into the framework, resulting in the low-crystallinity products. This was the reason why WM-MOFs presented higher weight loss and lower decompoition temperature. Time dependent ESI-MS measurements (Figure 2c) were also performed to verify acceleration of the hydrolysis. The reactants were stirred in a flask at 120 °C for different periods followed by filtration of the solutes from the mixture. Subsequent analysis by ESI-MS demonstrated that ZrL$_x$ existed at the beginning of the reaction. When the reaction time was prolonged to 15 min, peaks at m/z 450−600 corresponding to Zr$_3$L$_x$ appeared. The Zr$_6$L$_x$ related peaks were presented, and red precipitate was observed by the naked eye after 30 min (Figure S9). Low solubility of Zr$_6$L$_x$ clusters led to the weak intensity of the peaks. On the contrary, no obvious differences were found (Figure S10), and the solution was still clear after 30 min for the contrasts (Figure S9). In consideration of this phenomenon, we conclude that the cluster coordination and pore environment could be finely tuned through a competitive coordination strategy by introducing trace H$_2$O and modulating reagents, resulting in the visualized and well-ordered channels. Notably, the intact pore channels in MOFs are imaged by conventional TEM. We
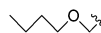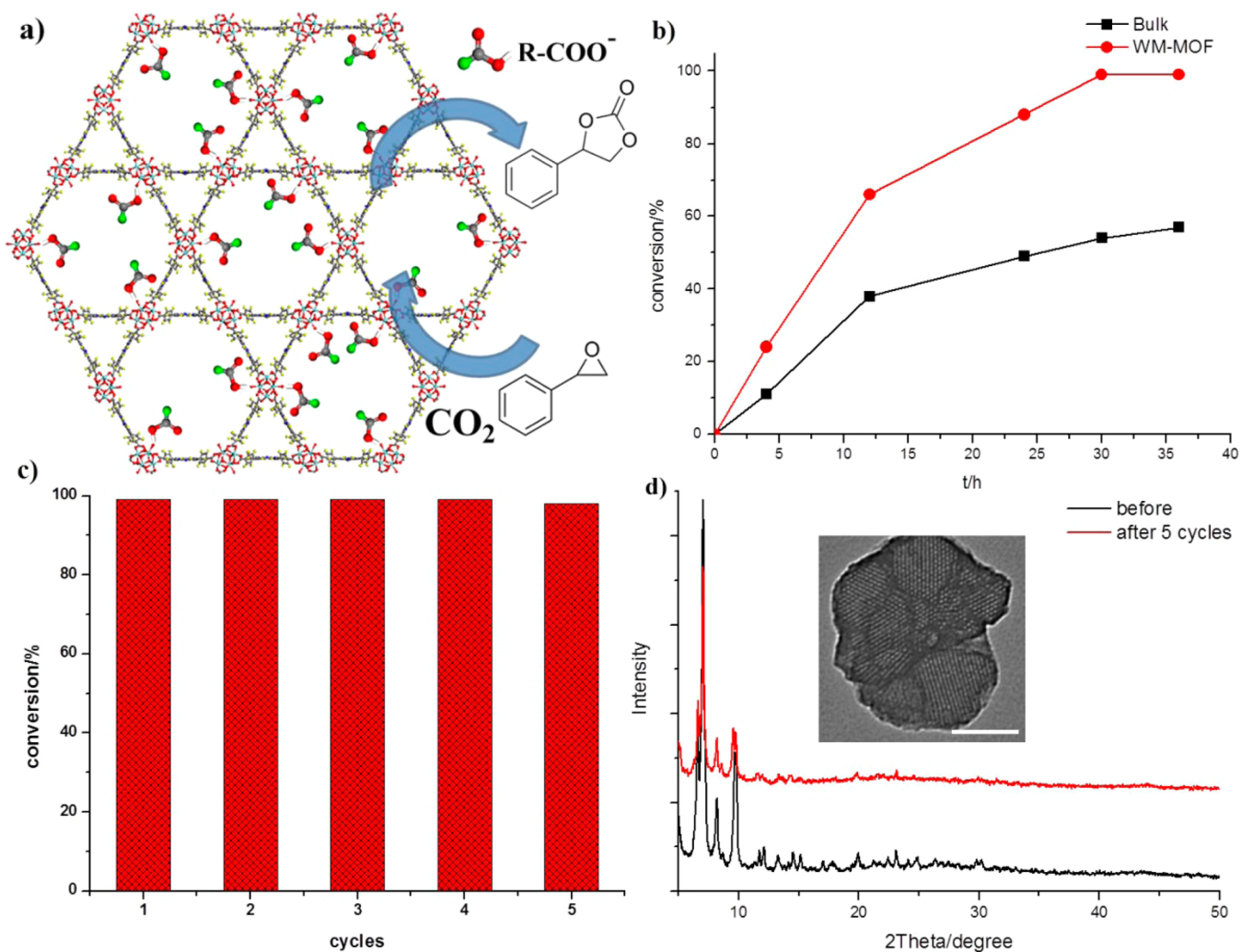
Figure 4. (a) Schematic representation of cycloaddition reaction of styrene oxide and CO_2 over WM-MOF. (b) Cycloaddition of CO_2 and styrene oxide with different catalysts. (c) Recycling study of WM-MOF. (d) PXRD patterns of WM-MOF before and after organic reaction (inset, TEM image of WM-MOF after organic reaction, scale bar 50 nm).

Table 1. Synthesis of Various Carbonates Catalyzed by WM-MOFs[a]

Entry	R-	T/°C	t/h	Conversion[b] /%	Selectivity[b] /%
1	Ph-	60	30	99	100
2	Me-	r.t[c]	24	96	94
3	Cl-	60	8	99	93
4	$\sim\!\sim\!\!O\!\!\sim$	60	16	96	100

[a]Reaction conditions: 17.5 mmol epoxide, 20 mg catalyst (0.34 mol % Zr), 5% TBAB, no solvent, CO_2 balloon. [b]Determined by GC-MS. [c]Room temperature.

speculate that tuning the pore environment of MOFs is a probable procedure to achieve intact structure of MOFs under TEM, which will have a significant impact on the further research of MOFs.

The facile synthetic procedure of WM-MOFs could be extended to other metallic−porphyrin systems, including single-metal-TCCP (Co-TCCP, Mn-TCCP, Fe-TCCP, and Cu-TCCP) and mixed-metal-TCCP (Ni_7Mn_3, Ni_3Co_7, Cu_7Fe_3, $Ni_5Co_3Fe_2$, and $Ni_4Co_2Fe_2Mn_2$), in which well-ordered mesoporous channels could also be clearly visualized in TEM images (Figures 3 and S11−S16). Interestingly, when other aliphatic carboxylic acids (formic acid, lauric acid, and oleic acid) were used as modulating reagents, WM-MOFs could also be fortunately achieved (Figures S17−S19). These structures were further characterized by XRD, SAXS, HAADF-STEM, BET, TGA, and ICP (Figures S20−S38 and Table S1).

Carbon dioxide (CO_2) is the primary source of greenhouse gas, causing enormous global energy and environmental problems. Chemical fixation of CO_2 to renewable chemical products would be an efficient route to overcome these issues. Up to now, a great number of catalysts[30−32] have been employed to convert CO_2 into cyclic carbonates which are used as aprotic polar solvents and electrolytes in batteries.[33,34] However, most of the processes demanded high pressures and temperatures, which greatly limited practical application.[30,31] Taking account of the structural advantage of WM-MOFs, we chose the fixation of carbon dioxide with epoxides to produce

five-membered cyclic carbonates as the model reaction (Figure 4a). We focused our initial research on the reaction of styrene oxide in the presence of n-Bu$_4$NBr (TBAB, 5 mol %) as cocatalyst at 60 °C under atmospheric pressure of CO$_2$. We were pleased to find the WM-MOF (0.34 mol % Zr) showed excellent catalytic performance after 30 h under solvent-free conditions (Table 1, entry 1, Figure S39). The substituent R could be both electron-withdrawing and electron-donating groups to afford the desired products in excellent conversion and selectivity (Table 1, entries 2−4) under corresponding temperature and time. To illuminate the relationship between structure and performance, control experiments were carried out (Figure 4b). Figure S40 showed that WM-MOFs possessed a slightly higher CO$_2$ uptake compared to that of bulk counterparts. The superior catalytic performance of WM-MOFs might be ascribed to (1) the competitive coordination of modulating reagent resulting in more exposed unsaturated Lewis acid catalytic sites in WM-MOFs or (2) the nanoscale of WM-MOFs being beneficial to mass diffusion. Impressively, other WM-MOFs also showed excellent catalytic performance for the reaction (Table S2). Furthermore, recycling use of WM-MOFs was carried out simply by separating the catalyst via centrifugation: the catalyst could maintain its structure and catalytic activity even after five successive catalytic cycles (Figure 4c). TEM and XRD results of the recycling catalyst (Figures 4d and S41) demonstrated that the morphology and structure of the catalyst were kept after the catalysis. The good reusability of WM-MOFs could obviously benefit its practical applications in the future.

CONCLUSIONS

In summary, we successfully developed a competitive coordination strategy to synthesize a series of stable and visualized WM-MOFs through fine-tuning pore environment. The long-range ordered channels are observed through conventional TEM. Fascinatingly, this general procedure can be extended to other single- and mix-metal-TCCP systems. The WM-MOFs show excellent catalytic performance for the cycloaddition of CO$_2$ and epoxides, which mainly comes from the unique structure, plenty of exposed catalytic sites, and fast mass diffusion. We believe that our strategy demonstrates a great potential in designing and synthesizing other nano-MOFs with tunable structure and improved performance.

ASSOCIATED CONTENT

Ⓢ Supporting Information

The Supporting Information is available free of charge on the ACS Publications website at DOI: 10.1021/acsami.7b06497.

> Materials, methods, and supporting figures (PDF)
> 2D HAADF-STEM images of WM-MOFs taken at consecutive tilt angles from 0 to −10° (AVI)
> 2D HAADF-STEM images of WM-MOFs taken at consecutive tilt angles from 0 to 10° (AVI)

AUTHOR INFORMATION

Corresponding Author
*E-mail: wangxun@mail.tsinghua.edu.cn.

ORCID Ⓘ
Xun Wang: 0000-0002-8066-4450

Notes
The authors declare no competing financial interest.

ABBREVIATIONS

WM-MOF, well-ordered mesoporous metal−organic framework
TEM, transmission electron microscopy
XRD, X-ray diffraction
TG, thermogravimetric
NMR, nuclear magnetic resonance
ESI-MS, electrospray ionization-mass spectrometry
TCPP, tetrakis(4-carboxyphenyl)-porphyrin
DMF, N,N-dimethylformamide
HAADF-STEM, high-angle annular dark-field scanning TEM
EDX, energy-dispersive X-ray spectroscopy
XPS, X-ray photoelectron spectra
SAXS, small-angle X-ray scattering
BET, Brunauer−Emmett−Teller
ICP-OES, inductively coupled plasma optical emission spectrometry
TBAB, tetrabutylammonium bromide

REFERENCES

(1) Li, H.; Eddaoudi, M.; O'Keeffe, M.; Yaghi, O. M. Design and Synthesis of an Exceptionally Stable and Highly Porous Metal-organic Framework. *Nature* **1999**, *402*, 276−279.

(2) Zhou, H.-C.; Long, J. R.; Yaghi, O. M. Introduction to Metal-organic Frameworks. *Chem. Rev.* **2012**, *112*, 673−674.

(3) Kitagawa, S.; Kitaura, R.; Noro, S. Functional Porous Coordination Polymers. *Angew. Chem., Int. Ed.* **2004**, *43*, 2334−2375.

(4) Rungtaweevoranit, B.; Zhao, Y.; Choi, K. M.; Yaghi, O. M. Cooperative Effects at the Interface of Nanocrystalline Metal-organic Frameworks. *Nano Res.* **2016**, *9*, 47−58.

(5) Liu, J.; Chen, L.; Cui, H.; Zhang, J.; Zhang, L.; Su, C.-Y. Applications of Metal-organic Frameworks in Heterogeneous Supramolecular Catalysis. *Chem. Soc. Rev.* **2014**, *43*, 6011−6061.

(6) Xu, X.; Lu, Y.; Yang, Y.; Nosheen, F.; Wang, X. Tuning the Growth of Metal-organic Framework Nanocrystals by Using Polyoxometalates as Coordination Modulators. *Sci. China Mater.* **2015**, *58*, 370−377.

(7) DeCoste, J. B.; Peterson, G. W. Metal-organic Frameworks for Air Purification of Toxic Chemicals. *Chem. Rev.* **2014**, *114*, 5695−5727.

(8) Sumida, K.; Rogow, D. L.; Mason, J. A.; McDonald, T. M.; Bloch, E. D.; Herm, Z. R.; Bae, T. H.; Long, J. R. Carbon Dioxide Capture in Metal-organic Frameworks. *Chem. Rev.* **2012**, *112*, 724−781.

(9) Horcajada, P.; Chalati, T.; Serre, C.; Gillet, B.; Sebrie, C.; Baati, T.; Eubank, J. F.; Heurtaux, D.; Clayette, P.; Kreuz, C.; Chang, J.; Hwang, Y. K.; Marsaud, V.; Bories, P.; Cynober, L.; Gil, S.; Férey, G.; Couvreur, P.; Gref, R. Porous Metal-organic-framework Nanoscale Carriers as a Potential Platform for Drug Delivery and Imaging. *Nat. Mater.* **2010**, *9*, 172−178.

(10) Zhang, J.-P.; Zhang, Y.-B.; Lin, J.-B.; Chen, X.-M. Metal Azolate Frameworks: From Crystal Engineering to Functional Materials. *Chem. Rev.* **2012**, *112*, 1001−1033.

(11) Ke, F.; Wang, L.; Zhu, J. Facile Fabrication of CdS-metal-organic Framework Nanocomposites with Enhanced Visible-light Photo-catalytic Activity for Organic Transformation. *Nano Res.* **2015**, *8*, 1834−1846.

(12) Li, S.; Huo, F. Metal-organic Framework Composites: from Fundamentals to Applications. *Nanoscale* **2015**, *7*, 7482−7501.

(13) Wu, S.; Zhu, Y.; Huo, Y.; Luo, Y.; Zhang, L.; Wan, Y.; Nan, B.; Cao, L.; Wang, Z.; Li, M.; Yang, M.; Cheng, H.; Lu, Z. Bimetallic Organic Frameworks Derived CuNi/Carbon Nanocomposites as

Effcient Electrocatalysts for Oxygen Reduction Reaction. *Sci. China Mater.* **2017**, DOI: 10.1007/s40843-017-9041-0.

(14) Xu, Z.; Zhang, W.; Weng, J.; Huang, W.; Tian, D.; Huo, F. Encapsulation of Metal Layers Within Metal-organic Frameworks as Hybrid Thin Films for Selective Catalysis. *Nano Res.* **2016**, *9*, 158−164.

(15) Cliffe, M. J.; Wan, W.; Zou, X.; Chater, P. A.; Kleppe, A. K.; Tucker, M. G.; Wilhelm, H.; Funnell, N. P.; Coudert, F.; Goodwin, A. L. Correlated Defect Nanoregions in a Metal-organic Framework. *Nat. Commun.* **2014**, *5*, 4176−1483.

(16) Wu, H.; Chua, Y. S.; Krungleviciute, V.; Tyagi, M.; Chen, P.; Yildirim, T.; Zhou, W. Unusual and Highly Tunable Missing-linker Defects in Zirconium Metal-organic Framework UiO-66 and Their Important Effects on Gas Adsorption. *J. Am. Chem. Soc.* **2013**, *135*, 10525−10532.

(17) Ameloot, R.; Vermoortele, F.; Hofkens, J.; De Schryver, F. C.; De Vos, D. E.; Roeffaers, M. B. J. Three-dimensional Visualization of Defects Formed During the Synthesis of Metal-organic Frameworks: a Fluorescence Microscopy Study. *Angew. Chem., Int. Ed.* **2013**, *52*, 401−405.

(18) Xiao, D. J.; Oktawiec, J.; Milner, P. J.; Long, J. R. Pore Environment Effects on Catalytic Cyclohexane Oxidation in Expanded Fe$_2$(dobdc) Analogues. *J. Am. Chem. Soc.* **2016**, *138*, 14371−14379.

(19) Islamoglu, T.; Goswami, S.; Li, Z.; Howarth, A. J.; Farha, O. K.; Hupp, J. T. Postsynthetic Tuning of Metal-organic Frameworks for Targeted Applications. *Acc. Chem. Res.* **2017**, *50*, 805−813.

(20) Vermoortele, F.; Bueken, B.; Le Bars, G.; Van de Voorde, B.; Vandichel, M.; Houthoofd, K.; Vimont, A.; Daturi, M.; Waroquier, M.; Van Speybroeck, V.; Kirschhock, C.; De Vos, D. E. Synthesis Modulation as a Tool to Increase the Catalytic Activity of Metal-organic Frameworks: the Unique Case of UiO-66(Zr). *J. Am. Chem. Soc.* **2013**, *135*, 11465−11468.

(21) Shearer, G. C.; Chavan, S.; Bordiga, S.; Svelle, S.; Olsbye, U.; Lillerud, K. P. Defect Engineering: Tuning the Porosity and Composition of the Metal-organic Framework UiO-66 *via* Modulated Synthesis. *Chem. Mater.* **2016**, *28*, 3749−3761.

(22) Shearer, G. C.; Chavan, S.; Ethiraj, J.; Vitillo, J. G.; Svelle, S.; Olsbye, U.; Lamberti, C.; Bordiga, S.; Lillerud, K. P. Tuned to Perfection: Ironing Out the Defects in Metal-organic Framework UiO-66. *Chem. Mater.* **2014**, *26*, 4068−4071.

(23) He, S.; Chen, Y.; Zhang, Z.; Ni, B.; He, W.; Wang, X. Competitive Coordination Strategy for the Synthesis of Hierarchical-pore Metal-organic Framework Nanostructures. *Chem. Sci.* **2016**, *7*, 7101−7105.

(24) Zhu, Y.; Ciston, J.; Zheng, B.; Miao, X.; Czarnik, C.; Pan, Y.; Sougrat, R.; Lai, Z.; Hsiung, C.; Yao, K.; Pinnau, I.; Pan, M.; Han, Y. Unravelling Surface and Interfacial Structures of a Metal-organic Framework by Transmission Electron Microscopy. *Nat. Mater.* **2017**, *16*, 532−536.

(25) Mayoral, A.; Sanchez-Sanchez, M.; Alfayate, A.; Perez-Pariente, J.; Diaz, I. Atomic Observations of Microporous Materials Highly Unstable under the Electron Beam: the Cases of Ti-doped AlPO$_4$-5 and Zn-MOF-74. *ChemCatChem* **2015**, *7*, 3719−3724.

(26) Lebedev, O. I.; Millange, F.; Serre, C.; Van Tendeloo, G.; Férey, G. First Direct Imaging of Giant Pores of the Metal-organic Framework MIL-101. *Chem. Mater.* **2005**, *17*, 6525−6527.

(27) Zhu, L.; Zhang, D.; Xue, M.; Li, H.; Qiu, S. Direct Observations of the MOF (UiO-66) Structure by Transmission Electron Microscopy. *CrystEngComm* **2013**, *15*, 9356−9359.

(28) Wiktor, C.; Turner, S.; Zacher, D.; Fischer, R. A.; Tendeloo, G. V. Imaging of Intact MOF-5 Nanocrystals by Advanced TEM at Liquid Nitrogen Temperature. *Microporous Mesoporous Mater.* **2012**, *162*, 131−135.

(29) Feng, D.; Gu, Z.-Y.; Li, J.-R.; Jiang, H.-L.; Wei, Z.; Zhou, H.-C. Zirconium-metalloporphyrin PCN-222: Mesoporous Metal-organic Frameworks with Ultrahigh Stability as Biomimetic Catalysts. *Angew. Chem., Int. Ed.* **2012**, *51*, 10307−10310.

(30) Song, Y.; Cheng, C.; Jing, H. Aza-crown Ether Complex Cation Ionic Liquids: Preparation and Applications in Organic Reactions. *Chem. - Eur. J.* **2014**, *20*, 12894−12900.

(31) Feng, D.; Chung, W.-C.; Wei, Z.; Gu, Z.-Y.; Jiang, H.-L.; Chen, Y.-P.; Darensbourg, D. J.; Zhou, H.-C. Construction of Ultrastable Porphyrin Zr Metal-organic Frameworks through Linker Elimination. *J. Am. Chem. Soc.* **2013**, *135*, 17105−17110.

(32) Liu, L.; Zhang, J.; Fang, H.; Chen, L.; Su, C.-Y. Metal-organic Gel Material Based on UiO-66-NH$_2$ Nanoparticles for Improved Adsorption and Conversion of Carbon Dioxide. *Chem. - Asian J.* **2016**, *11*, 2278−2283.

(33) Schäffner, B.; Schäffner, F.; Verevkin, S. P.; Börner, A. Organic Carbonates as Solvents in Synthesis and Catalysis. *Chem. Rev.* **2010**, *110*, 4554−4581.

(34) He, H.; Perman, J. A.; Zhu, G.; Ma, S. Metal-organic Frameworks for CO$_2$ Chemical Transformations. *Small* **2016**, *12*, 6309−6324.